Proceedings of the ASME 2011 Conference on Smart Materials, Adaptive Structures and Intelligent Systems
SMASIS2011
September 18-21, 2011, Scottsdale, Arizona, USA

SMASIS2011-5226

LASER WELDING OF NICKEL TITANIUM AND 304 STAINLESS STEEL TUBES

Ryan Hahnlen
Smart Materials and Structures Lab
Dept. of Mechanical Engineering
The Ohio State University
Columbus, Ohio 43210
Email: hahnlen.1@osu.edu

Gordon Fox
Smart Materials and Structures Lab
Dept. of Mechanical Engineering
The Ohio State University
Columbus, Ohio 43210
Email: fox.483@osu.edu

Marcelo J. Dapino*
Smart Materials and Structures Lab
Dept. of Mechanical Engineering
The Ohio State University
Columbus, Ohio 43210
Email: dapino.1@osu.edu

ABSTRACT

Shape memory nickel-titanium (NiTi) can generate large blocking stresses and high recovery strains, up to 8%, which make NiTi a good candidate for solid state actuators, resulting in substantial weight and space savings when they replace traditional electric or hydraulic systems. A challenge surrounding NiTi based actuators is integration of the NiTi components into a given system; this alloy is difficult and expensive to machine and weld to itself and structural materials. In this research, we join NiTi and 304 stainless steel tubes 9.52 mm (0.375 in) in diameter through laser welding to create joints with weld depths up to 1650 μ*m (0.065 in). By joining NiTi to a common structural material that is easily machined and readily welded to other materials, the challenges surrounding system integration are reduced. The joints prepared in this study were characterized through optical microscopy, hardness mapping, and mechanical testing. The average ultimate shear strength of these joints is 423 MPa (61.3 ksi) and the resulting HAZ has a maximum width of* 21.9 μ*m with a maximum hardness of 929 HV.*

INTRODUCTION

NiTi is a shape memory alloy capable of recovering large deformations, up to 8% [1,2], and exerting large forces as it undergoes a temperature induced transformation from its martensite to austenite phase. These properties make NiTi a desirable material for use in solid state actuators with reduced weight, moving parts, and complexity for a wide variety of applications. However, the broad implementation of NiTi in commercial products has been hindered by difficulties in the integration of these alloys into structural systems.

Machining NiTi has proven to be difficult due to its high ductility, work hardening characteristics, and non-linear stress-strain behavior. These characteristics can cause poor surface finish, irregular chip breakage, and high tool wear [3]. The build-up of heat in traditional machining processes can also locally affect thermo-mechanical properties of the NiTi work piece, reducing the magnitude and repeatability of the shape memory effect [4]. Electric discharge machining is commonly used to create NiTi parts, however this process is relatively expensive when compared to traditional machining processes. Much of the expense of using NiTi can be eliminated if a reliable and efficient way of joining it to traditional structural materials, such as steel alloys, is used; however, joining NiTi to itself and dissimilar materials presents several challenges.

When fusion welding NiTi, there are two main concerns. The first is the loss of cold work and material training, which negatively influences the shape memory and superelastic effects, of the NiTi component due to excessive heating. It is possible to regain some of the original behaviors through post weld heat treatments and additional training, but this adds cost and complexity to the joining process [5]. In this study we avoid the issue of significant training loss through laser welding, a fusion welding process which utilizes a directed laser beam to heat and melt the base metal of the work pieces. The key benefit to laser welding over traditional fusion welding methods is the focused heat source which results in a narrow Heat Affected Zone (HAZ)

*Address all correspondence to this author.

and less thermally affected material. This characteristic of laser welding helps to alleviate the loss of shape memory properties without needing post weld treatments. NiTi has been successfully welded to itself [6, 7] and dissimilar metals [8] using this process with the resulting joint maintaining shape memory or superelastic properties comparable to that of the non-welded base metal. One drawback to laser welding is the relatively low penetration of the resulting welds, as this process is generally limited to joint penetration of approximately 1 mm.

The second concern in welding NiTi is the formation of brittle intermetallic compounds. Fusion welding NiTi to itself can result in solidification or "hot cracking". Hot cracking occurs due to solidification temperature range of an alloy. As the molten NiTi in a weld pool cools through its solidification range, a network of solid alloy forms in the liquid portion of the weld pool which is usually $TiNi_2$, a brittle compound. When the solidifying compounds begin to form grain structures, the liquid $TiNi_2$ infiltrates the grain boundaries. As the liquid cools and solidifies the additional shrinking leaves cracks at the grain boundaries. These serve as crack initiation sites that can propagate through the weld and cause joint failure. In severe cases, the weld may fail completely as it cools after the initial welding process [5, 9].

"Cold cracking" is a phenomenon that occurs when joining titanium alloys to ferrous alloys. The titanium and iron form brittle intermetallic compounds, such as TiFe and $TiFe_2$, which have low strength at room temperature [4]. Fusion welding NiTi to steel readily creates these intermetallics which form along the weld line [10]. The contracting volume of the work piece places the intermetallics phases under stress and causes cracks to propagate during cooling. These cracks often result in total weld failure as the joint cools to room temperature. As described by Hall [11], a NiTi/ferrous alloy weld can be successfully made with Ni-rich filler metal. The addition of Ni dilutes the weld pool, reducing the relative amount of molten Ti and Fe in the joint, hence avoiding the formation of intermetallic compounds. By adding more Ni to the weld pool, there is also a reduction in hot cracking due to relative reduction of molten Ti.

This research focuses on laser welding NiTi to 304 stainless steel (304 SS) tubes for use in torsional solid-state actuators. This particular stainless steel alloy was chosen as the structural material because it is easy to machine and weld [12]. By joining NiTi to a structural material, the difficulties and cost associated with its use and integration are substantially diminished. Intermetallic formation is suppressed through the use of a Ni-rich filler metal. The resulting joints are characterized through optical microscopy, hardness testing, and mechanical testing to determine their torsional strength.

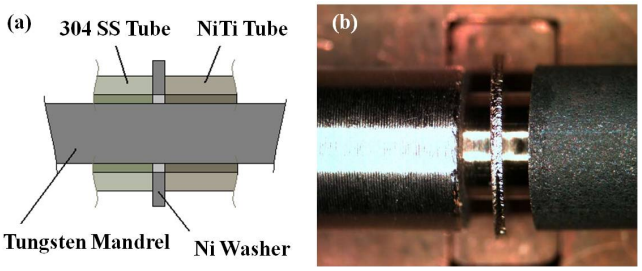

Figure 1. (a) CUTAWAY DIAGRAM OF ASSEMEBELED NiTi/304 SS PILOT SAMPLE; (b) PILOT JOINT PRIOR TO WELDING.

EXPERIMENTAL PROCEEDURE

Sample Construction

Three types of joints, differing by their diameters and wall thicknesses, were created for this research. All were welded using a neodymium-doped yttrium aluminum garnet (Nd:YAG) laser. The Ni-rich filler metal was commercially pure nickel (Ni 200) which took different forms as needed for each type of joint. To avoid reactions with oxygen, nitrogen, or other atmospheric contaminants, argon was used as a shielding gas in all cases.

The first joint geometry utilized small diameter NiTi and 304 SS tubes with 5.08 mm (0.200 in) outer diameters and 813 μm (0.032 in) thick walls. These pilot samples were used to determine the maximum single-pass weld penetration attainable with the laser system. The pilot joints were created by holding a 381 μm (0.015 in) thick Ni washer between the NiTi and 304 SS tubes, as seen in Figure 1, and rotating the sample as the laser pulsed. The tungsten mandrel was used to keep all components in place and aligned during welding. Pilot joints were sectioned for optical microscopy to observe weld penetration and the associated HAZ in the NiTi base metal. For each pilot trial, the spot size, peak power, and pulse frequency were fixed at 1.1 mm, 1.8 kW, and 0.7 pulses per second (pps), respectively, while total pulse energy was varied by changing pulse length. Parameters for these joints are presented in Table 1.

A second set of joints were created utilizing 9.53 mm (0.375 in) diameter tubes with 381 μm thick walls. Five total samples were made, four of which were tested for torsional strength while the fifth was used for optical microscopy in order to observe the weld penetration and the resulting HAZ. The Ni filler used in these joints took the form of pre-placed unions, shown in Figure 2 (a). An assembled joint before welding is shown in Figure 2 (b). For each trial, the spot size, peak power, and pulse frequency were fixed at 0.7 mm, 1.1 kW, and 1.3 pps, respectively. Pulse energy was varied by adjusting pulse duration. All parameters can be seen in Table 1. Thin-walled samples 3, 4, and 5 have the same weld parameters, as discussed later.

A third set of samples were created by using 9.53 mm diameter NiTi and 304 SS tubes with 1.65 mm (0.065 in) thick walls.

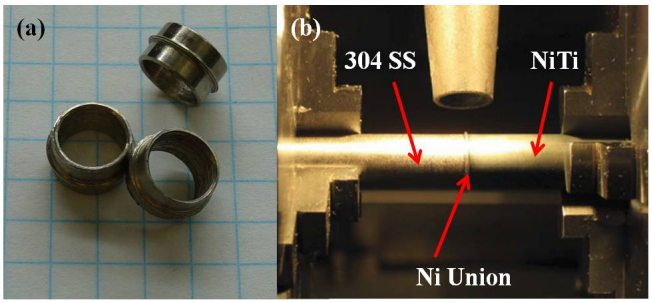

Figure 2. (a) Ni UNIONS USED FOR FILLER METAL IN THIN-WALLED NiTi/304 SS LASER WELDS; (b) ASSEMBELED THIN-WALLED SAMPLE PRIOR TO WELDING.

This set of joints was created by forming a 45° bevel on the mating ends of each tube and making multiple weld passes to fill the groove, similar to methods for creating large-scale pipe welds. A pre-weld setup can be seen in Figure 3. The Ni filler for this joint configuration was hand-fed 254 μm (0.010 in) diameter Ni wire when welding the root passes and 508 μm (0.020 in) diameter Ni wire for welding the fill passes. A total of four thick-walled samples were created, three of which were used for optical microscopy and one was tested for torsional strength. Since this welding process required multiple passes, more heat was applied to the NiTi tube in the thick-walled joints. For this reason, along with possible variation due to hand-feeding the Ni filler, most of the samples were used for optical microscopy to observe possible weld defects and the formation of a HAZ. Two sets of parameters were used in creating each thick-walled sample, one for the initial root pass and the other for subsequent fill passes. The spot size was set at 0.4 mm for the root passes and 0.75 mm for fill passes. Pulse frequency for each pass was fixed at 5 pps. All parameters for both passes are shown in Table 1

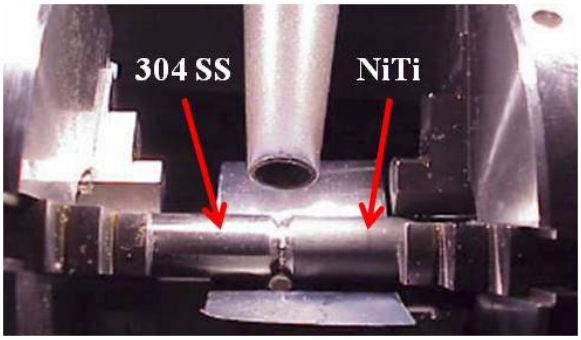

Figure 3. WELD SETUP OF NiTi/304 SS THICK-WALLED JOINT SHOWING INITIAL ROOT PASS AND AIR DAM.

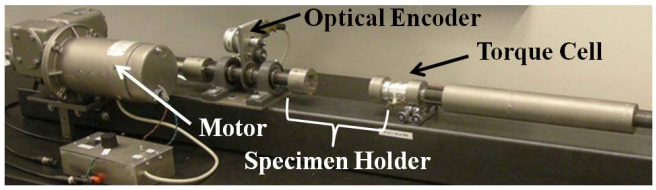

Figure 4. TORSION SYSTEM USED FOR MECHANICAL TESTING OF THIN AND THICK-WALLED NiTi/304 SS LASER WELDED SAMPLES.

Optical Microscopy and Hardness Testing

All pilot samples, thin-walled sample 5, and thick-walled samples 1 through 3 were sectioned and polished for optical microscopy studies. Through microscopy, weld penetration and HAZ width were determined. Weld penetration and HAZ widths were measured using ImageJ [13], an image processing program. For all samples, the HAZ is a clearly visible lightly shaded region adjacent to and running parallel with the weld pool boundary in the NiTi portion of the sample.

In addition to observing weld penetration and possible HAZ regions, hardness maps were made from thin-walled sample 5 and thick-walled sample 1. The hardness maps were constructed by making a series of indents with a diamond indenter and 25 gram load spaced 200 μm in both the axial (X-axis) and radial (Y-axis) directions. These maps were used to determine bulk NiTi hardness and observe possible large scale HAZ formation. To augment the hardness maps and investigate the possible HAZ regions observed in the optical micrographs, individual hardness tests were conducted using a diamond indenter and 10 gram load.

Mechanical Testing

Thin-walled samples 1 through 4 and thick-walled sample 4 were used for mechanical testing to observe the ultimate torsional strength of the welds. For all tests, a torsional testing system, shown in Figure 4, was used to apply an angular displacement ramp at a rate of $0.5^\circ/\text{sec}$. Samples were loaded until failure while applied torque was measured with a reaction torque cell and angular displacement of the sample was measured using a optical angular encoder. For each test, clamp grips were used to fixture the specimen. The edge of the grips was placed 6.35 mm (0.25 in) from the centerline of the weld so each test had the same length of NiTi and 304 SS tube deflecting with applied load.

RESULTS AND DISCUSSION

Sample Construction

The sectioned pilot samples do not show instances of cracking at the toes or faces of the welds. This indicates that there was sufficient Ni filler metal to dilute the weld pool and avoid the formation of Ti-Fe intermetallics. There is no discoloration of the base metals which is an indication of over heating. A completed

Table 1. LASER PARAMETERS FOR NiTi/304 SS SAMPLE CONSTRUCTION.

Type	Specimen	Spot Size [mm]	Pulse Frequency [pps]	Peak Power [kW]	Pulse Duration [ms]	Pulse Energy [J]
Pilot Test	1	1.10	0.7	1.80	9.8	17.64
	2	1.10	0.7	1.80	12.0	21.60
	3	1.10	0.7	1.80	14.0	25.20
Thin Wall	1	0.7	1.3	1.25	14.0	17.50
	2	0.70	1.3	1.15	13.0	14.95
	3	0.70	1.3	1.10	13.0	14.30
	4	0.70	1.3	1.10	13.0	14.30
	5	0.70	1.3	1.10	13.0	14.30
Thick Wall	Root	0.40	5.0	0.52	3.4	1.77
	Fill	0.75	5.0	1.00	13.0	13.00

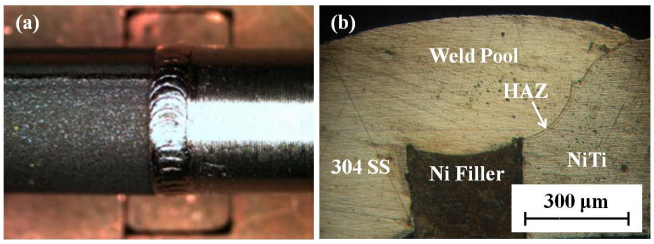

Figure 5. NiTi/304 SS PILOT JOINT (a) AFTER WELDING; (b) MICROGRAPH AFTER SECTIONING AND POLISHING.

Figure 6. COMPLETED THIN-WALLED NiTi/304 SS SPECIMENS; INSET: DETAIL OF WELD REGION IN SAMPLE 1 SHOWING DISCOLORATION INDICATIVE OF EXCESSIVE BASE METAL HEATING.

pilot test sample is shown in Figure 5 (a).

The welded thin-walled samples are seen in Figure 6. In thin-walled sample 1, the 304 SS portion has a discolored region which is highlighted in the inset. This is an indication of excessive heating of the joint. Subsequent thin-walled samples were made with lower pulse energies to avoid overheating the base metals. From Table 1, samples 3, 4, and 5 were constructed using the same parameters. This is because in creating sample 3, a pinhole defect was observed in the weld bead. The defect is likely due to surface contamination on either the base metal or Ni insert. To obtain a surface-defect free joint with the same parameters, sample 4 was made. Sample 5 was made to observe the microsection resulting from the parameter set used in samples 3 and 4.

Completed thick-walled samples, seen in Figure 7, have no visible surface defects. The slight differences in bead formation are due to hand feeding the Ni filler wire during welding. Initial root passes in the thick-walled joints were crack sensitive and occasionally cracked as the weld cooled. The subsequent fill passes became much less crack sensitive. This is believed to be due to the proximity of the NiTi and 304 SS tubes at the root and the relatively small size of Ni filler that was used for the root pass. As fill passes continue, the groove geometry provided greater separation of NiTi and 304 SS, thereby reducing the risk for Ti-Fe intermetallic formation.

The depth of the joint in the thick-walled samples represents a method of overcoming the primary limitation of laser welding, relatively shallow weld penetration. By using multiple passes, the joint depth is essentially unlimited. To decrease the time required to create such joints and increase repeatability, the wire feed process could be automated for future joints.

Optical Microscopy

Optical microscopy of the pilot samples reveals an average weld penetration of 457 μm (0.018 in). Also present in the micrographs is a lighter shaded region in the NiTi base metal adjacent to the weld pool, as seen in Figure 5 (b). This region is visible in all pilot samples even without surface etching and is believed to represent the HAZ in the NiTi tube. Using ImageJ, the width of

Figure 7. COMPLETED THICK-WALLED NiTi/304 SS SPECIMENS.

Weld	Depth [μm]	HAZ Width [μm]	Pulse Energy [J]
1	432	7.01	17.6
2	432	10.7	21.6
3	483	13.0	25.2

Table 2. LASER WELD PENETRATION AND PULSE ENERGY OF PILOT NiTi/304 SS SAMPLES.

this region was measured at several points along the NiTi boundary of the weld pool. The average of these measurements for each sample and the maximum weld penetration is reported in Table 2.

The pulse energy of the laser can be estimated by multiplying the peak power by the pulse length for each sample. In order to attain greater penetration, more energy must be applied to the joint. While the ideal weld would have full penetration and a small HAZ, these are conflicting objectives. In comparing the pulse energy to the penetration measured in the pilot samples in Table 2, there is little increase in penetration as pulse energy increases, but there is a significant increase in the width of the optically observed HAZ. For this reason, the pulse energy in pilot sample 1 is preferred and was used as a starting point in creating the thin-walled joints.

A micrograph of thin-walled specimen 5 is shown in Figure 8 (a). Penetration extends into the annular cylinder of the Ni union, as expected from the average penetration of the pilot tests. A light shaded region is observed in the NiTi region adjacent to the weld pool. The average thickness of this region is 7.90 μm which falls within the range of values observed in the pilot samples.

Results from the thick-walled sectioned samples are shown in Table 3. The thick-walled specimens have full thickness weld penetration, 1.65 mm, as designed by the joint setup and weld procedure, and an average HAZ extension of 21.9 μm. This is wider than the optical HAZ identified in the pilot and thin-walled

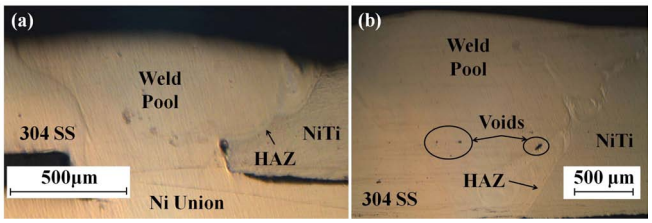

Figure 8. MICROGRAPH OF (a) THIN-WALLED NiTi/304 SS SPECIMEN 5; (b) THICK-WALLED NiTi/304 SS SPECIMEN 1.

Weld	HAZ Width [μm]
1	19.2
2	24.4
3	22.2

Table 3. AVERGAE HAZ EXTENSION OBSERVED IN THICK-WALLED NiTi/304 SS SAMPLES.

joints. The increase in HAZ width is expected as multiple weld passes cause increased heating of the base metals with each successive pass.

The thick-walled joint sections show that although some cracking in the root pass was observed, subsequent welds remelted the root pass and further diluted the weld pool which prevented the reformation of the cracks. This can be seen in Figure 8 (b). The micrographs of the thick-walled joints show voids in some welds. The voids are characterized as round or oblong dark areas in the sections and are differentiated from cracks by the smooth corners as opposed to sharp jagged features seen in crack formations. The voids are due to contaminates in the weld from either the tube beveling process or the hand-fed Ni filler wire. As the joint is heated to create fusion of the base metals, the contaminants vaporize and produce a gas bubble within the solidifying weld pool [14]. While such a defect would not be acceptable in production welds, it is easily remedied by ensuring all workpieces and filler material are thoroughly cleaned prior to joining.

Hardness Testing

The hardness map created from thin-walled sample 5 is shown in Figure 9. On the right portion of the map there is a lighter colored region which corresponds to the boundary of the weld pool and NiTi tube. In this region, the map shows a contiguous region of increased hardness, between 400 and 800 HV. To the right of the light colored region is the NiTi tube which has a hardness range of approximately 200 to 350 HV. This hardness value is typical of NiTi [15] and indicates that the material in this region is unaffected by the heat generated by the welding pro-

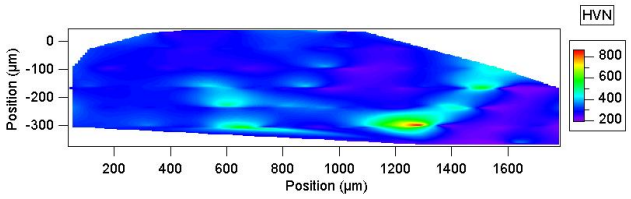

Figure 9. HARDNESS MAP OF THIN WALL NiTi/304 SS THIN-WALLED LASER WELD SPECIMEN 5.

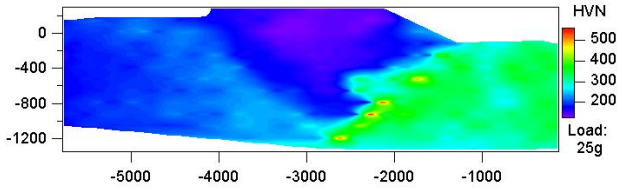

Figure 10. HARDNESS MAP OF THIN WALL NiTi/304 SS THICK-WALLED LASER WELD JOINT 1.

cess. The variation in hardness of the bulk NiTi is likely due to different orientations of the martensitic variants.

A similar map made from thick-walled specimen 1 is shown in Figure 10. The NiTi tube to the far right has a hardness that ranges from 200 to 350 HV. There is a region in the NiTi tube adjacent to the weld pool that has isolated hardened areas, but no continuous HAZ is indicated on the map.

While the hardness maps do indicate regions of increased hardness in the NiTi tube immediately adjacent to the weld pools, the spacing of the measurement points is too wide to measure the hardness of the regions identified through optical microscopy. In order to investigate the optically identified regions and determine if they constitute the NiTi HAZ, additional hardness indents were created. The additional measurements taken on thin-walled specimen 5 are shown in Figure 11. Two indents are completely within the optically identified HAZ, indicated for clarity by the dashed curved lines. For reference, a single indent was made in both the bulk NiTi and the solidified weld pool. The NiTi indent has a hardness of 213 HV and is 47 μm from the weld pool boundary. Both indents within the HAZ have significantly higher hardness values, 929 and 898 HV. From a weld pool indent close to the HAZ boundary, the hardness drops to 521 HV. Both non-HAZ indents indicate that the hardness observed in the HAZ is limited to the region observed through optical microscopy.

Similar analysis was conducted on thick-walled specimen 1. Two indents were made within the optically identified HAZ and have hardness values of 801 and 757 HV, as seen in Figure 12. A reference indent in the bulk NiTi 38 μm away from the weld line

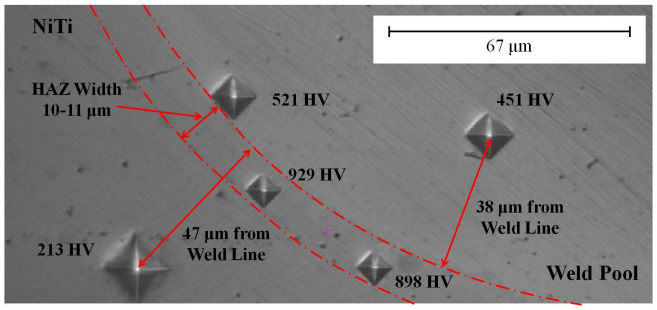

Figure 11. INDIVIDUAL HARDNESS MEASUREMENTS IN OPTICALLY IDENTIFIED HAZ OF NiTi/304 SS THIN-WALLED SPECIMEN 5.

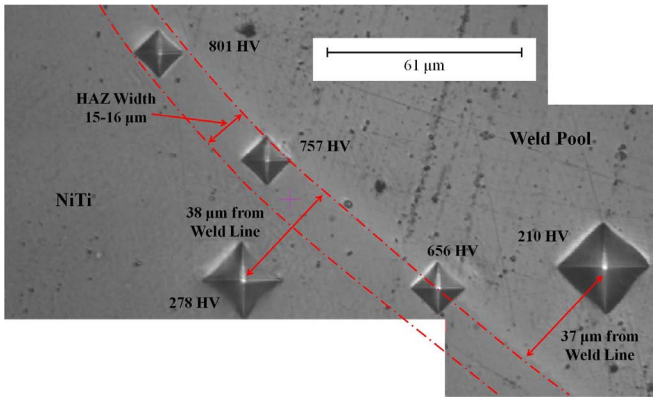

Figure 12. COMPOSITE IMAGE OF INDIVIDUAL HARDNESS MEASUREMENTS IN OPTICALLY IDENTIFIED HAZ OF NiTi/304 SS THICK-WALLED SPECIMEN 1.

has a hardness of 278 HV, indicating that the HAZ is within the limits identified through optical microscopy. In both the thick and thin-walled hardness measurements, the HAZ in the NiTi tube is limited to a narrow region at the weld interface. Because of this, the welding process should have little effect on the total shape memory effect of the NiTi tube.

Mechanical Testing

Torque-angle plots for thin-walled samples 1 through 4 are shown in Figure 13. The ultimate torques for each sample were found and used to calculate the ultimate shear stresses at the outer fiber:

$$\tau = \frac{T r_o}{J} \tag{1}$$

where

$$J = \frac{\pi}{2}\left(r_o^2 - r_i^2\right) \tag{2}$$

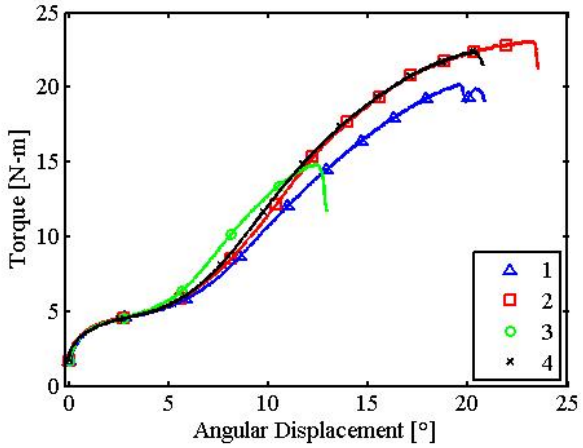

Figure 13. TORQUE-ANGLE PLOTS OF THICK-WALLED NiTi/304 SS SAMPLES.

Sample	Ult. Torque [N-m]	Ult. Shear Stress [MPa]
1	20.3	423
2	23.2	481
3	15.0	312
4	22.5	467

Table 4. THIN-WALLED NiTi/304 SS LASER WELD SAMPLE STRENGTH TESTING RESULTS.

and r_o and r_i are the outer and inner radii, respectively. A summary of the ultimate torques and stresses is shown in Table 4.

Thin-walled samples 1, 2, and 4 have similar ultimate stresses while the ultimate stress of sample 3 is significantly lower. The lower strength of sample 3 is due to the weld defects noted previously. The pinhole defects in sample 3 act as stress concentration points and are the source of early failure. Similar to voids observed in the thick-walled sample sections, pinhole defects are caused by contaminants on the base metal surfaces or filler metal. Thin-walled sample 4 was created using the same parameters as sample 3 in response to seeing the surface defects in the previous sample. Therefore, sample 3 can be treated as an outlier in statistically analyzing the strength of the thin-walled samples. The average ultimate shear strength of samples 1, 2, and 4 is 457 MPa with a standard deviation of 30.6 MPa and coefficient of variance, $C_v = s/\bar{\tau}$, where s is the standard deviation and $\bar{\tau}$ is the average ultimate shear strength, of 6.7%. This indicates that the strength of the thin-walled specimens was not strongly affected by the variation in pulse energy used in welding.

The characteristic behavior of NiTi is observed in Figure 13. Four distinct regions are present: an initially elastic region which corresponds to the linear loading of twined martensite; a detwinned region characterized by a lower torque-angle slope; a second linear elastic region corresponding to the elastic loading of detwinned martensite; and a plastic deformation region which leads to specimen failure. The detwinning plateau is characterized by a change in slope of the load-displacement plots due to the large deformations induced by detwinning of the martensitic crystalline structure. Detwining occurs as NiTi is loaded between its critical start and finish stresses. Using linear regression of the initial elastic region, detwinning region, and second linear region, the critical start and finish torques were found at the intersection points of the linearly extrapolated segments. Using the critical torques and equations (1) and (2), the critical stresses were calculated. For all four thin-walled samples, the average critical start and finish stresses are 80.7 MPa and 118 MPa, respectively. There is very little variation in the critical stresses of the thin-walled specimens. A summary of the critical torques and stresses can be seen in Table 5.

Thick-walled sample 4 was tested to observe its torsional strength. The torque-angle plot for thick-walled sample 4 can be seen in Figure 14. From the plot there is a maximum torque of 48.0 N-m which corresponds to an ultimate shear strength of 346 MPa. This is slightly lower than the average shear stress found from the thin-walled tubes and is believed to be due to the presence of voids observed in the micrographs of thick-walled samples 1, 2, and 3.

From the plot the critical start torque was determined to be 13.1 N-m which corresponds to 94.5 MPa. There is no clearly defined critical finish torque due to the thick wall of the NiTi tube. In the thin-walled tubes, shear stress has very little variation through the tube wall whereas the thick-walled tube exhibits a larger stress gradient through the tube wall. In consequence, NiTi at the outer surface may be completely detwinned while NiTi at the inner radius of the tube may have yet to reach the critical start stress. While there may not be complete detwinning through the NiTi tube cross-section, NiTi that is partially detwinned will generate recovery stresses and recover induced strain as it is heated above its austenite start temperature.

In all tests, the torsion samples failed at the weld toe on the NiTi tube. This corresponds with the location of the HAZ observed in the micrographs. In all cases, the 304 SS tube exhibits plastic deformation indicating that the weld strength is greater than the yield strength of the structural tube.

CONCLUDING REMARKS

In this research we have studied three different laser welded joints between NiTi and 304 SS tubes. In constructing the joints, the formation of intermetallic Ti-Fe compounds that typically cause NiTi/ferrous alloy welds to have low strength were suppressed by using Ni filler metal to dilute the weld pool and pre-

Sample	Crit. Start Torque [N-m]	Crit. Finish Torque [N-m]	Crit. Start Stress [MPa]	Crit. Finish Stress [MPa]
1	4.11	5.55	85.5	115
2	3.84	5.87	80.0	122
3	3.83	5.66	79.3	118
4	3.74	5.57	77.9	116
Avg.	3.88	5.66	80.7	118
S.D.	0.161	0.144	3.33	3.10
C_v	4.1%	2.6%	4.1%	2.6%

Table 5. THIN-WALLED NiTi/304 SS LASER WELD SAMPLE CRITICAL TORQUES AND STRESSES.

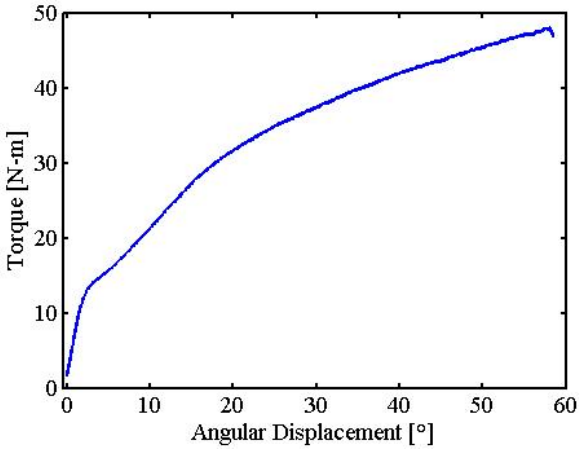

Figure 14. TORQUE-ANGLE PLOT OF THICK-WALLED NiTi/304 SS SAMPLE 4.

vent widespread alloying of Ti and Fe. In examining the pilot joints, it was found that increasing the pulse energy provides little increase in weld penetration but does result in an increase the HAZ width. Maximum weld penetration and extension of the HAZ in the pilot samples are 483 μm and 13.1 μm, respectively.

Based upon the findings from the pilot study, thin-walled NiTi and 304 SS tubes were used to make full penetration butt welds 381 μm thick. These samples were used for optical microscopy and hardness studies as well as torsional testing to determine the welds' ultimate shear strength. Optical microscopy revealed that the average HAZ extension in the thin-walled samples is 7.90 μm. Hardness mapping and individual hardness tests indicate that outside of the HAZ identified through optical microscopy, the NiTi tube remains unaffected by the laser welding process and as such, should maintain its shape memory properties. Maximum observed hardness is 929 HV which was found within the identified HAZ. Mechanical testing results show that the average ultimate shear strength of the thin-wall welds is 457 MPa, sufficient to completely detwin the NiTi tube and plastically deform the 304 SS tube.

A multi-pass process was used to obtain full penetration welds in NiTi and 304 SS tubes with 1.65 mm wall thickness. These samples represent a significant increase in the weld depth typically observed in laser welding applications and present a method for creating structural joints of arbitrary depth while maintaining the primary benefit of laser welding, a small HAZ. While the weld sections were free of intermetallic based cracking, there were some defects due to contaminates within the weld pool. Similar to the thin-walled tubes, a HAZ was observed in the NiTi tube that extended, on average, 21.9 μm beyond the weld pool. Maximum hardness measurements, up to 801 HV, were found within the identified HAZ. Hardness mapping indicates that NiTi outside of the optically observed HAZ is unaffected by welding. The ultimate shear strength of thick-walled specimen 4 is 346 MPa. This value is slightly lower than that observed in the thin-walled specimen but the lower strength is attributed to voids observed in the other thick-walled samples. The strength of the thick-walled weld is sufficient to begin detwinning of NiTi and cause plastic deformation of the 304 SS tube.

The results show that laser welding is a viable process for joining NiTi to 304 SS for use in solid-state actuators. The process affects only a small amount of the joined NiTi, and with the addition of Ni filler metal, nearly eliminates the formation of adverse intermetallic compounds and cold cracking. The resulting strength of the joints is high enough to allow for the generation of blocking forces or strain recovery and is not the limiting factor in the joint systems that were studied.

ACKNOWLEDGMENT

The authors would like to thank The Boeing Company, particularly Jim Mabe and Tad Calkins, working through the Smart Vehicle Concept Center (www.mecheng.osu.edu/svc), a National Science Foundation Industry/University Cooperative Research Center Program (I/UCRC), for its technical and financial sup-

port of this research. The authors also thank Tim Frech and Jay Eastman from the Edison Welding Institute for their assistance in preparing the samples, Suresh Babu and Tapasvi Lolla from the Ohio State University Materials Science and Engineering Department for assistance with hardness measurements, and the Smart Vehicle Concepts Graduate Fellowship Program.

REFERENCES

[1] Johnson Matthey, 2011. Nitinol technical specifications: Transformation, physical, electrical, magnetic and mechanical. Website: `http://jmmedical.com`.

[2] Nitinol Devices & Components, 2010. Material data sheet: Nitinol SM495 wire. Website: `http://www.nitinol.com`.

[3] Weinert, K., and Petzoldt, V., 2004. "Machining of niti based shape memory alloys". *Materials Science and Engineering A,* ***378***, pp. 180–184.

[4] Wu, M., 2001. "Fabrication of Nitinol materials and components". In Proceedings of the International Conference on Shape Memory and Superelastic Technologies, pp. 258–292.

[5] Wang, G., 1997. "Welding of Nitinol to stainless steel". In Proceedings of the International Conference on Shape Memory and Super Elastic Technologies, pp. 131–136.

[6] Falvo, A., Furgiuele, F., and Maletta, C., 2005. "Laser welding of a NiTi alloy: Mechanical and shape memory behaviour". *Materials Science and Engineering A,* ***412***, pp. 235–240.

[7] Kahn, M. I., Panda, S. K., and Zhou, Y., 2008. Effects of welding parameters on the mechanical performance of laser welded Nitinol.

[8] Gugel, H., Schuermann, A., and Theisen, W. T., 2006. Laser welding of NiTi wires.

[9] Cieslak, M. J., 1993. *ASM Handbook: Volume 6: Welding, Brazing, and Soldering*. ASM International.

[10] van der Eijk, C., Fostervoll, H., Sallom, Z., and Akselsen, O., 2003. "Plasma welding of NiTi to NiTi, stainless steel and Hastelloy c276". In Conference proceedings ASM Materials Solutions.

[11] Hall, P., 2005. US Patent 6875949: Method of welding titanium and titanium based alloys to ferrous metals, April.

[12] AK Steel Corporation, 2007. 304/304L stainless steel. Website: `http://www.aksteel.com`.

[13] US National Institutes of Health. ImageJ. Website: `http://rsbweb.nih.gov/ij`.

[14] Hobart Institute of Welding Technology, 2009. *Welding Guide*. Hobart Institute of Welding Technology, Troy, OH.

[15] Alapati, S., Brantley, W., Nusstein, J., Daehn, G., Svec, T., Powers, J., Johnston, W., and Gou, W., 2006. Vickers hardness investigation of work-hardening in used NiTi rotary instruments.